

Trapped-particle diocotron modes

T. J. Hilsabeck and T. M. O'Neil

Department of Physics, University of California at San Diego, La Jolla, California 92093

(Received 18 March 2003; accepted 16 June 2003)

Recent experiments have characterized trapped-particle modes on a non-neutral plasma column [A. A. Kabantsev, C. F. Driscoll, T. J. Hilsabeck, T. M. O'Neil, and J. H. Yu, *Phys. Rev. Lett.* **87**, 225002 (2001)], and in this paper we present a theoretical model of the modes. Theoretical predictions for the mode frequency, damping rate, and eigenmode structure are compared to experimental observation. The modes are excited on a non-neutral plasma column in which classes of trapped and passing particles have been created by the application of a potential barrier. The column resides in a Malmberg–Penning trap, and the barrier is created by applying a voltage to an azimuthally symmetric section of the wall near the axial mid-point of the column. Low energy particles near the edge of the column (where the barrier is strong) are trapped in one end or the other, while high energy particles near the center of the column transit the entire length. The modes have azimuthal variation $\ell = 1, 2, \dots$, and odd z -symmetry. The trapped particles on either side of the barrier execute $\mathbf{E} \times \mathbf{B}$ drift oscillations producing density perturbations that are 180° out of phase with each other, while passing particles run back and forth along the field lines attempting to Debye shield the perturbed charge density. The mode is damped by collisional scattering across the separatrix between trapped and passing particles. The damping rate is calculated using a boundary layer analysis of the Fokker–Planck equation. It is also shown that the damping is associated with the radial transport of plasma particles. © 2003 American Institute of Physics.
[DOI: 10.1063/1.1599356]

I. INTRODUCTION

Electric and magnetic field inhomogeneities in plasma containment devices cause a fraction of the particles to remain localized in certain regions. This condition gives rise to a class of low frequency electrostatic oscillations known as trapped-particle modes.² In these modes, trapped particles remain isolated from the global mode structure and experience $\mathbf{E} \times \mathbf{B}$ drift oscillations locally, while passing particles stream along the field lines Debye shielding the trapped-particle charge density perturbations. In this sense, trapped-particle modes resemble drift waves wherein the trapped particles play the role of ions and passing particles the role of electrons. Trapped-particle modes were originally investigated for toroidal geometry, but have been predicted for and observed in other geometries, such as the Columbia Linear Machine.³

Recent experiments with magnetically confined non-neutral plasma columns have characterized a new trapped-particle mode: the trapped-particle diocotron mode.¹ In this paper we provide a theoretical description of the mode, and compare theoretical prediction to experimental measurement for the frequency, damping rate, and eigenmode structure. The agreement is good (for example, 10% percent for frequency and 50% percent for the damping rate) over a substantial range of experimental parameters.

The modes are excited on a non-neutral (pure electron) plasma column to which an azimuthally symmetric potential barrier has been applied creating classes of trapped and passing particles. This electrostatic barrier, the squeeze voltage, is typically applied near the axial mid-point of the column.

Particles with low axial velocity are then trapped in either end, while high axial velocity particles pass back and forth over the full length of the column.

The mode dynamics is easy to understand. Trapped particles in the two ends of the column undergo low frequency $\mathbf{E} \times \mathbf{B}$ drift oscillations that are 180° out of phase with each other, while passing particles move back and forth along the magnetic field lines Debye shielding the charge perturbation of the trapped particles.

The mode damping is due to collisional scattering of marginally trapped particles. Following the analysis of Rosenbluth, Ross, and Kostomarov⁴ for the dissipative trapped-ion mode, we solve the Fokker–Planck equation in a thin boundary layer near the separatrix between trapped and passing particles, and find that the relative damping scales like $\sqrt{\nu/\omega}$, rather than ν/ω . Here, ν is the collision frequency, ω is the mode frequency, and the square root is important because ν/ω is small.

To understand why collisions have an enhanced effect near the separatrix, first note that the trapped and passing particles experience very different dynamics. In the absence of collisions, the perturbed velocity distributions for the trapped and passing particles would be discontinuous (in value and slope) at the separatrix. Small angle scattering, described by the Fokker–Planck collision operator, is essential in smoothing the discontinuity. Steep gradients in a narrow boundary layer enhance the effective collision frequency to the point where an order unity correction (the smoothing) is made to the perturbed velocity distribution.

Significantly, the correction contains a component that is

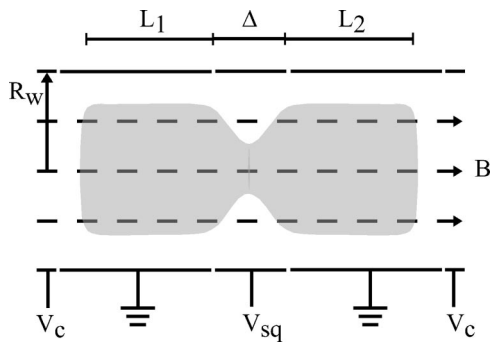


FIG. 1. A pure electron plasma column confined in a Malmberg–Penning trap that has been partially divided by the application of an external squeeze voltage, V_{sq} . End cylinders are maintained at negative potentials to provide axial confinement, while radial confinement is provided by a large axial magnetic field $\mathbf{B} = B\hat{z}$.

in phase with the mode electric field, so the mode can exchange energy with the scattered particles. The dominant energy exchange occurs because the mode transports the scattered particles radially outward. The liberated electrostatic energy increases the mode energy, and would cause growth of a positive energy mode. However, the observed trapped-particle diocotron mode has negative energy, so the mode damps.

A direct experimental test was made to verify that scattering of marginally trapped particles causes the damping. The scattering rate was enhanced artificially by applying a potential that oscillates in resonance with the axial bounce motion of marginally trapped particles. The damping rate was observed to increase an order of magnitude coincident with the application of this oscillation potential.

The remainder of the paper is organized as follows. In Sec. II we describe the confinement geometry and plasma equilibrium. In Sec. III we discuss the basic equations for the mode dynamics. In Sec. IV we solve for the mode frequency and eigenmode structure in the absence of collisions. An analytic solution is possible in an idealized limit, but a numerical solution is necessary for a realistic density profile and potential barrier profile. In Sec. V, the effect of collisions is included, and the damping rate is calculated. In Sec. VI we discuss Landau resonances and argue that Landau (and bounce resonant) damping are typically small for these modes.

II. CONFINEMENT GEOMETRY AND EQUILIBRIUM

The pure electron plasma column is confined in a Malmberg–Penning trap configuration as shown schematically in Fig. 1. The confinement region is bounded radially by a series of conducting cylinders of radius R_w . The end cylinders are held at negative potential to provide axial confinement of the electron plasma, while radial confinement is provided by a large axial magnetic field $\mathbf{B} = B\hat{z}$. Here, (r, θ, z) is a cylindrical coordinate system with the z -axis coincident with the axis of the cylindrical wall. Because the column is unneutralized, there is a radial space charge electric field and consequent $\mathbf{E} \times \mathbf{B}$ drift rotation of the column.

A static, θ -symmetric barrier is created by applying a negative voltage (the “squeeze” potential) to a short cylindrical section of the bounding wall. The resulting barrier potential is an increasing function of radius, with more particles trapped near the radial edge of the plasma than near the trap axis. At any given radius, the squeeze potential presents an insurmountable barrier to low axial velocity particles, trapping them in the end regions. Particles with high axial velocity pass over the squeeze potential and sample the entire length of the column.

In the experiments, the plasma has time to come into thermal equilibrium along each field line before the mode is launched. Thus, the equilibrium distribution function is given by

$$f_0(r, z, v) = \frac{N(r) \exp\left\{-\frac{1}{T}[mv^2/2 - e\phi_0(r, z)]\right\}}{\int dz \int dv \exp\left\{-\frac{1}{T}[mv^2/2 - e\phi_0(r, z)]\right\}}, \tag{1}$$

where v is the z -component of the velocity. The transverse velocity components have been integrated out, anticipating that drift dynamics will be used in the description of the mode. The z -integrated density $N(r)$ and the temperature on the axis [i.e., $T(r=0)$] are known from measurement. The temperature is assumed to be independent of r for simplicity and for want of better knowledge. The possibility of introducing error here will be discussed later (see Sec. V). The self-consistent equilibrium potential $\phi_0(r, z)$ is obtained by substituting the charge density $-en_0(r, z) = -e \int dv f_0(r, z, v)$ into Poisson’s equation and numerically solving subject to the known boundary conditions for the potential on the trap wall.

In Fig. 2, equilibrium density and potential contours are shown for a typical case. The z -integrated density profile, $N(r)$, is monotonically decreasing with a peak of $8.2 \times 10^8 \text{ cm}^{-2}$ on axis. The plasma temperature in this example is 1 eV and the end ring potentials are -100 V . A -20 V squeeze potential is applied over a central conducting ring of length 7 cm. The radial wall of the trap is located at 3.5 cm. The equilibrium solution in Fig. 2 demonstrates the effectiveness of the Debye shielding in forcing the potential and density to be z -independent, except in the squeeze region and near the ends of the column. This condition holds generally for the plasmas under consideration in this paper.

Figure 3 shows phase space orbits executed by particles moving along a particular magnetic field line (at $r = 0.5 \text{ cm}$) in the equilibrium of Fig. 2. All of the particles are reflected by the large confinement fields at the ends. Particles whose maximum axial velocity is less than the separatrix velocity ($0.68\bar{v}$ for this field line) are reflected by the squeeze barrier and are trapped in the ends. Orbits for the trapped particles are shown as dashed curves. Particles with a high axial energy pass through the squeeze region and sample the entire length of the column during a bounce orbit. The passing particle orbits are shown as the solid curves in Fig. 3.

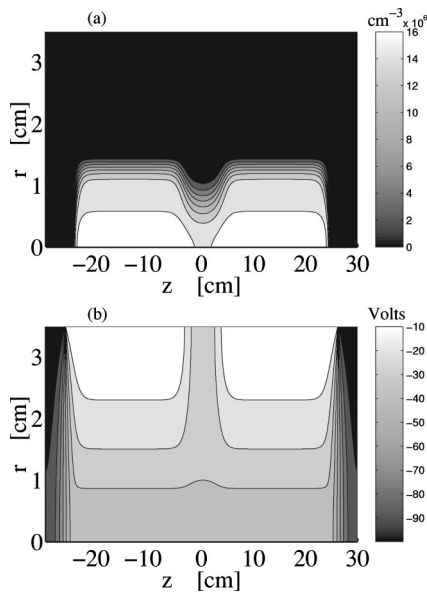


FIG. 2. Density (a) and potential (b) contours for a squeezed column equilibrium. A -20 V squeeze potential has been applied to a 7 cm ring at the axial midpoint of the plasma. It is clear that axial variations in density and potential are shielded out of the two main parts of the column ($6 \text{ cm} \leq |z| \leq 24 \text{ cm}$).

The separatrix velocity is determined indirectly from the experimental measurements. The electric potential inside the trap is obtained using the Poisson–Boltzmann solution described above. Debye shielding produces a potential that is axially uniform inside the plasma on either side of the squeeze region. In the squeeze region, the potential varies smoothly and reaches a maximum at $z=0$. The energy barrier seen by a particle bouncing at a radius r is determined by the difference in the potential between the region of smooth potential (say, $z = \pm 15 \text{ cm}$) and the center of the squeeze region ($z=0 \text{ cm}$). Particles with a maximum kinetic energy that matches this potential energy barrier are moving at the separatrix velocity,

$$v_s(r) = \left\{ \frac{2e}{m} [\phi_0(r,15) - \phi_0(r,0)] \right\}^{1/2}. \tag{2}$$

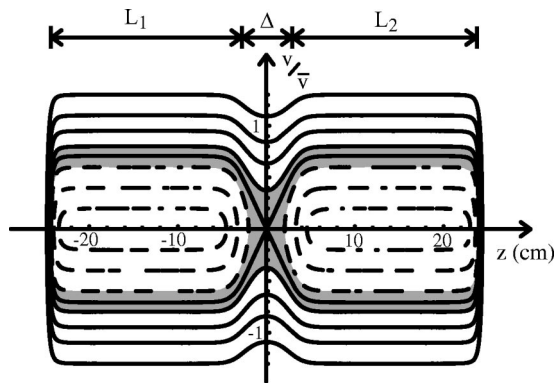


FIG. 3. Phase-space orbits at $r=0.5 \text{ cm}$ with an applied squeeze potential $V_{sq} \sim \phi_0(0,0)/2$. Trapped orbits are dashed lines and passing orbits are solid. A particle on the separatrix orbit has maximum velocity of $0.68\bar{v}$. The shaded region represents the boundary layer (not to scale) where velocity space diffusion occurs and causes mode damping.

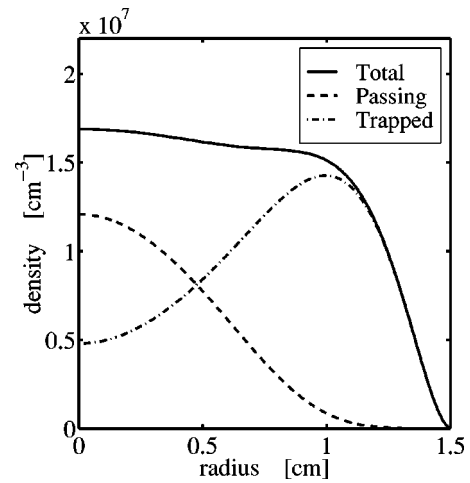


FIG. 4. Trapped, passing and total particle density profiles. The externally applied squeeze potential results in more trapped particles near the radial edge of the plasma and more passing particles near the trap axis.

Because the barrier potential is strongest nearest the trap wall, the separatrix velocity is an increasing function of radius.

The density profiles of trapped and passing particles at any given radius can be determined from the total particle density profile $n_0(r)$ and the separatrix velocity $v_s(r)$. The density of particles trapped by the squeeze barrier at a particular radius is

$$n_t(r) = \int_{-v_s(r)}^{v_s(r)} dv f_0(r,15,v) = n_0(r) \operatorname{erf} \left[\frac{v_s(r)}{\sqrt{2}\bar{v}} \right], \tag{3}$$

and the passing density is $n_p(r) = n_0(r) - n_t(r)$. Figure 4 shows the trapped, passing, and total density profiles for the equilibrium of Fig. 2, and clearly demonstrates the radial dependence of the fraction of trapped particles.

The Debye shielding of the squeeze potential results in a barrier that is a strong function of radius. Most particles near the edge of the plasma are trapped and most particles near the trapped axis are passing. The radial localization of trapping is a general feature of externally applied electrostatic squeeze potentials.

III. DYNAMICAL EQUATIONS

Because the cyclotron frequency is the largest of the relevant dynamical frequencies and the cyclotron radius is the smallest of the length scales, the mode dynamics can be described by the drift kinetic equation,

$$\left(\frac{\partial}{\partial t} + v \frac{\partial}{\partial z} - \frac{c}{Br} \frac{\partial \phi}{\partial \theta} \frac{\partial}{\partial r} + \frac{c}{Br} \frac{\partial \phi}{\partial r} \frac{\partial}{\partial \theta} + \frac{e}{m} \frac{\partial \phi}{\partial z} \frac{\partial}{\partial v} \right) f = C(f), \tag{4}$$

where $f = f(r, \theta, z, v, t)$ is the distribution of guiding centers and $\phi(r, \theta, z, t)$ is the electric potential. Of course, $\phi(r, \theta, z, t)$ is determined by $f(r, \theta, z, v, t)$ through Poisson’s equation and the known boundary conditions for ϕ on the

wall. On the right hand side, $C(f)$ is the Fokker–Planck collision operator integrated over the velocity components transverse to $\mathbf{B} = B\hat{z}$.⁵

Although equilibrium distribution (1) was written down using thermal equilibrium considerations, not surprisingly it is a time independent solution of Eq. (4). This follows from the fact that $C(f_0) = 0$, $\partial\phi_0/\partial\theta = \partial f_0/\partial\theta = 0$, and $v\partial f_0/\partial z + (e/m)(\partial\phi_0/\partial z)(\partial f_0/\partial z) = 0$.

We take the mode perturbation to be small and linearize Eq. (4) in $\delta f = f - f_0$ and $\delta\phi = \phi - \phi_0$. The result is

$$\left(\frac{\partial}{\partial t} + v \frac{\partial}{\partial z} + \omega_E \frac{\partial}{\partial \theta} + \frac{e}{m} \frac{\partial \phi_0}{\partial z} \frac{\partial}{\partial v} - C \right) \delta f = - \frac{e}{m} \frac{\partial f_0}{\partial v} \frac{\partial \delta \phi}{\partial z} + \frac{c}{Br} \frac{\partial f_0}{\partial r} \frac{\partial \delta \phi}{\partial \theta}, \quad (5)$$

where $\omega_E = (c/Br)(\partial\phi_0/\partial r)$ is the $\mathbf{E} \times \mathbf{B}$ drift rotation frequency for the equilibrium. Since f_0 and ϕ_0 are independent of θ and t , we consider perturbations of the form

$$(\delta f, \delta \phi) = (\delta f_\ell, \delta \phi_\ell) \exp(i\ell\theta - i\omega t). \quad (6)$$

Equation (5) then reduces to the form

$$\left(-i\omega + i\ell\omega_E + v \frac{\partial}{\partial z} + \frac{e}{m} \frac{\partial \phi_0}{\partial z} \frac{\partial}{\partial v} - C \right) \delta f_\ell = - \frac{e}{m} \frac{\partial \delta \phi_\ell}{\partial z} \frac{\partial f_0}{\partial v} + \frac{ic\ell}{Br} \frac{\partial f_0}{\partial r} \delta \phi_\ell. \quad (7)$$

The left hand side of Eq. (7) includes the term $C(\delta f_\ell)$, which is the linearization of the Fokker–Planck collision operator with respect to the perturbation δf_ℓ . The linearization includes four terms:

$$C(\delta f_\ell) = \frac{\partial}{\partial v} \left[D(v) \frac{\partial \delta f_\ell}{\partial v} + F(v) \delta f_\ell \right] + \frac{\partial}{\partial v} \left[\delta D(v) \frac{\partial f_0}{\partial v} + \delta F(v) f_0 \right], \quad (8)$$

where $D(v)$ and $F(v)$ are the parallel diffusion and drag coefficients evaluated for the equilibrium distribution f_0 , and $\delta D(v)$ and $\delta F(v)$ are the diffusion and drag coefficients evaluated for the perturbed distribution δf_ℓ . For future reference, note that any perturbation of the form $\delta h_\ell = g(r, z) f_0$ is such that $C(\delta h_\ell) = 0$. Also, note that near the separatrix, where derivatives of δf_ℓ are very large, only the highest derivative term in $C(\delta f_\ell)$ need be retained. In the separatrix boundary layer, Eq. (8) may be approximated by

$$C(\delta f_\ell) \approx D(v_s) \frac{\partial^2 \delta f_\ell}{\partial v^2}. \quad (9)$$

The parallel diffusion coefficient is of order $D \sim \nu \bar{v}^2$, but more accurately is given by

$$D(v_s) = \frac{8\sqrt{\pi} e^4 n T \Lambda}{m^3 v_s^3} \int_0^{mv_s^2/2T} \sqrt{t} e^{-t} dt, \quad (10)$$

where $\Lambda = \ln(r_c/b)$ is the Coulomb logarithm for the case where $e^2/T \equiv b \ll r_c \ll \lambda_D$.⁶

The justification of the linearization is subtle and requires some discussion. As mentioned, we will find that the mode damping is dominated by particles in a thin boundary layer near the separatrix. However, a nonlinear effect of the mode potential shifts the velocity of the separatrix up and down by an amount $\delta v_{nl} \sim e\delta\phi/mv_s$ every cycle. Particles in this band undergo a complicated sequence of trapping and detraping transitions that is missed by the linearized equation (7). Why then is the linearization valid, and what is the criterion for validity?

The essential point is that small angle scattering, which is included in Eq. (7), causes rapid trapping and detraping transitions over a broader velocity band than δv_{nl} . The effective collision frequency for scattering over the velocity interval δv_s is $\nu_{\text{eff}} = D(v_s)/(\delta v_s)^2$, where $D(v_s)$ is the parallel diffusion coefficient discussed above. One can understand this relation as the statement that velocity diffusion extends over the range δv_s during the time ν_{eff}^{-1} [i.e., $(\delta v_s)^2 = D\nu_{\text{eff}}^{-1}$]. For the scattering transitions across the separatrix to be at least as fast as the nonlinearity induced transitions, we set $\nu_{\text{eff}} = \omega' \equiv |\omega - \ell\omega_E|$, the Doppler shifted mode frequency as seen by a particle. This yields the collision dominated width $\delta v_s = \sqrt{D/\omega'} \approx \bar{v} \sqrt{\nu/\omega'}$, where the approximation $D \approx \nu \bar{v}^2$ has been used. In Sec. V, we will find that this is the width of the boundary layer that dominates mode damping. Thus, the criterion for validity of the linearization is the inequality $\delta v_s \gg \delta v_{nl}$, which can be written as $\sqrt{\nu/\omega'} \gg e\delta\phi/T$, where we have set $v_s \approx \sqrt{T/m}$.

IV. FREQUENCY AND EIGENMODE

In this section, we solve for the mode frequency and eigenmode structure. Both are described adequately by collisionless theory. The effect of weak collisions will be included in the next section, which discusses the mode damping.

The solution relies on the frequency ordering $\omega_b \gg \omega_E, \omega$, where $\omega_b = \pi\bar{v}/L$ is the characteristic axial bounce frequency for electrons and $L = L_1 + \Delta + L_2$ is the overall column length (see Fig. 1). Since ω and ω_E both scale like $1/B$, an expansion in the small parameter $\omega/\omega_b \sim \omega_E/\omega_b \ll 1$ is equivalently an expansion in $1/B$.

In zeroth order, Eq. (7) reduces to

$$\left(v \frac{\partial}{\partial z} + \frac{e}{m} \frac{\partial \phi_0}{\partial z} \frac{\partial}{\partial v} \right) \delta f_\ell = \frac{e}{T} v \frac{\partial \delta \phi_\ell}{\partial z} f_0, \quad (11)$$

where $C(\delta f_\ell)$ has been neglected and use has been made of $\partial f_0/\partial v = -(mv/T)f_0$ on the right hand side. Equation (11) can be rewritten as

$$\left(v \frac{\partial}{\partial z} + \frac{e}{m} \frac{\partial \phi_0}{\partial z} \frac{\partial}{\partial v} \right) \left(\delta f_\ell - \frac{e\delta\phi_\ell}{T} f_0 \right) = 0, \quad (12)$$

which is a statement that the quantity $[\delta f_\ell - (e\delta\phi_\ell/T)f_0]$ is constant along a bounce orbit. Thus, we may equate the value of this quantity to its bounce-average value, obtaining the result

$$\delta f_\ell = \langle \delta f_\ell \rangle + \frac{e}{T} [\delta\phi_\ell - \langle \delta\phi_\ell \rangle] f_0. \quad (13)$$

Here, the bracket indicates a bounce-average,

$$\langle g \rangle(r, \theta, \epsilon) = \frac{\oint \frac{dz}{v(z, \epsilon)} g[r, \theta, z, v(z, \epsilon)]}{\oint \frac{dz}{v(z, \epsilon)}}, \quad (14)$$

where $mv^2/2 - e\phi_0(r, z) = \epsilon$ specifies the orbit. In writing Eq. (13), use was made of the fact that f_0 is constant along an orbit.

To obtain an equation for $\langle \delta f_\ell \rangle$, we bounce-average Eq. (7) projecting out the zeroth order terms. The remaining (first order) terms describe cross magnetic field drift motion,

$$-i\omega \langle \delta f_\ell \rangle + i\ell \langle \omega_E \delta f_\ell \rangle = \frac{ic\ell}{Br} \left\langle \delta \phi_\ell \frac{\partial f_0}{\partial r} \right\rangle. \quad (15)$$

The second term on the right hand side of Eq. (13) specifies the distribution of electrons along a bounce orbit. This type of response, called an adiabatic response, gives rise to Debye shielding. Thus, we anticipate here, and verify *a posteriori* (see Sec. VI), that Debye shielding forces the mode potential to be z -independent, except in the region of the squeeze potential and near the ends of the column.

As a simple model that captures the essential physics, we use a step function approximation for the mode potential,

$$\delta \phi_\ell(r, z) = \begin{cases} \delta \phi_{\ell 1}(r), & 0 < z < L_1, \\ \delta \phi_{\ell 2}(r), & L_2 < z < 0, \end{cases} \quad (16)$$

where L_1 and L_2 are the lengths of the two trapped-particle regions (see Fig. 1). Likewise, we neglect the small but finite axial extent of the squeeze region and end when evaluating the bounce averages. The model assumes that the trapped-particle regions are long compared to the squeeze region and ends. The advantage of the model is that a partial differential eigenmode equation for $\delta \phi_\ell(r, z)$ is reduced to two coupled ordinary differential equations for $\delta \phi_{\ell 1}$ and $\delta \phi_{\ell 2}$. We will see that a simple physically motivated guess as to the ratio $\delta \phi_{\ell 1} / \delta \phi_{\ell 2}$ decouples these equations leaving a single ODE eigenmode equation.

The step function model simplifies the evaluation of bounce-averages. For trapped particles on side j ($j = 1$ or 2), the bounce-average mode potential is given by $\langle \delta \phi_\ell \rangle = \delta \phi_{\ell j}$, and for passing particles it is given by

$$\langle \delta \phi_\ell \rangle = \frac{L_1 \delta \phi_{\ell 1} + L_2 \delta \phi_{\ell 2}}{L_1 + L_2}. \quad (17)$$

Since the squeeze region and ends are neglected, the bounce-average products in Eq. (15) simplify: $\langle \omega_E \delta f_\ell \rangle = \omega_E \langle \delta f_\ell \rangle$ and $\langle \delta \phi_\ell \partial f_0 / \partial r \rangle = \langle \delta \phi_\ell \rangle \partial f_0 / \partial r$.

Equations (13) and (15) then imply that the perturbed distribution for trapped particles on the side j is given by

$$\delta f_{\ell j}^{(t)} = \frac{c\ell}{Br} \frac{\delta \phi_{\ell j}}{\omega'} \frac{\partial f_0}{\partial r}, \quad (18)$$

where $\omega'(r) \equiv \ell \omega_E(r) - \omega$. Likewise, the perturbed distribution for passing particles on side j is given by

$$\delta f_{\ell j}^{(p)} = \frac{c\ell}{Br} \frac{\langle \delta \phi_\ell \rangle}{\omega'} \frac{\partial f_0}{\partial r} + \frac{e}{T} [\delta \phi_{\ell j} - \langle \delta \phi_\ell \rangle] f_0, \quad (19)$$

where $\langle \delta \phi_\ell \rangle$ is given by Eq. (17).

The next step is to determine the density perturbations associated with trapped and with passing particles. Because the separatrix velocity is a function of radius [i.e., $v_s = v_s(r)$], one must be careful not to miscount particles. First consider the trapped particles. Equation (18) can be understood as implying that each trapped particle undergoes a radial step $\delta r_{\ell j} = -c\ell \delta \phi_{\ell j} / Br\omega'$, so that

$$\delta f_{\ell j}^{(t)}(r, v) = f^{(t)}(r - \delta r_{\ell j}, v) - f^{(t)}(r, v) = \frac{c\ell \delta \phi_{\ell j}}{Br\omega'} \frac{\partial f^{(t)}}{\partial r}. \quad (20)$$

Thus, the perturbation in the trapped-particle charge density is given by

$$\begin{aligned} \delta n_{\ell j}^{(t)}(r) &= \int_{-v_s(r - \delta r_{\ell j})}^{-v_s(r - \delta r_{\ell j})} dv f^{(t)}(r - \delta r_{\ell j}, v) \\ &\quad - \int_{-v_s(r)}^{-v_s(r)} dv f^{(t)}(r, v), \end{aligned} \quad (21)$$

which for small $\delta r_{\ell j}$ takes the form

$$\delta n_{\ell j}^{(t)}(r) = \int_{-v_s(r)}^{-v_s(r)} dv \delta f_{\ell j}^{(t)}(r, v) + 2 \frac{\partial v_s}{\partial r} \delta r_{\ell j} f^{(t)}(r, v_s). \quad (22)$$

Omission of the second term would miscount the number of trapped particles. Combining the two terms in Eq. (22) yields the result

$$\delta n_{\ell j}^{(t)} = \frac{c\ell}{Br} \frac{\delta \phi_{\ell j}}{\omega'} \frac{\partial n_t}{\partial r}, \quad (23)$$

where $n_t(r)$ is defined in Eq. (3). Of course, this result can be obtained more directly using a fluid theory for the trapped particles. Similar arguments for the passing particles yield the perturbed density,

$$\delta n_{\ell j}^{(p)} = \frac{c\ell}{Br} \frac{\langle \delta \phi_\ell \rangle}{\omega'} \frac{\partial n_p}{\partial r} + \frac{e}{T} [\delta \phi_{\ell j} - \langle \delta \phi_\ell \rangle] n_p, \quad (24)$$

where $n_p(r) = 2 \int_{v_s(r)}^\infty dv f_0(r, v)$.

Substituting density perturbations (23) and (24) into Poisson’s equation yields two coupled differential equations,

$$\begin{aligned} \frac{1}{r} \frac{\partial}{\partial r} \left(r \frac{\partial}{\partial r} \delta \phi_{\ell j} \right) - \frac{\ell^2}{r^2} \delta \phi_{\ell j} &= \frac{4\pi e c \ell}{Br} \frac{\delta \phi_{\ell j}}{\omega'} \frac{\partial n_t}{\partial r} + \frac{4\pi e c \ell}{Br} \frac{\langle \delta \phi_\ell \rangle}{\omega'} \frac{\partial n_p}{\partial r} \\ &\quad + \frac{4\pi e^2 n_p}{T} [\delta \phi_{\ell j} - \langle \delta \phi_\ell \rangle], \end{aligned} \quad (25)$$

for $\delta \phi_{\ell j}$ ($j = 1$ and 2). Two ratios of $\delta \phi_{\ell 1}(r) / \delta \phi_{\ell 2}(r)$ for which the equations decouple are easy to guess. For the choice $\delta \phi_{\ell 1}(r) = \delta \phi_{\ell 2}(r) = \langle \delta \phi \rangle$, the two equations each reduce to the usual eigenmode equation for a diocotron mode

$$\frac{1}{r} \frac{\partial}{\partial r} \left(r \frac{\partial}{\partial r} \delta \phi_{\ell j} \right) - \frac{\ell^2}{r^2} \delta \phi_{\ell j} = \frac{4\pi e c \ell}{Br} \frac{\delta \phi_{\ell j}}{\omega'} \frac{\partial n_0}{\partial r}, \quad (26)$$

where $n_0(r) = n_t(r) + n_p(r)$. In this case, two in-phase diocotron modes exist on the two sides of the barrier.

For the choice $L_1 \delta\phi_{\ell 1} = -L_2 \delta\phi_{\ell 2}$, Eq. (17) implies that $\langle \delta\phi_\ell \rangle = 0$ so the two equations each reduce to the form

$$\frac{1}{r} \frac{\partial}{\partial r} \left(r \frac{\partial}{\partial r} \delta\phi_{\ell j} \right) - \frac{\ell^2}{r^2} \delta\phi_{\ell j} = \frac{4\pi e c \ell}{Br} \frac{\delta\phi_{\ell j}}{\omega'} \frac{\partial n_t}{\partial r} + \frac{4\pi e^2 n_p}{T} \delta\phi_{\ell j}. \quad (27)$$

This is the eigenmode equation for the trapped-particle diocotron mode (or more precisely, modes). From the right hand side, one can see that trapped particles undergo $\mathbf{E} \times \mathbf{B}$ drift motion locally and passing particles stream along field lines attempting to Debye shield the perturbed charge density of the trapped particles. The condition $L_1 \delta\phi_{\ell 1} = -L_2 \delta\phi_{\ell 2}$ guarantees that the passing particle charge needed for shielding on one side of the barrier is exactly liberated on the other side. The equations must be solved subject to the boundary conditions $\delta\phi_{\ell j}(0) = \delta\phi_{\ell j}(R_w) = 0$.

An analytic solution of Eq. (27) can be obtained in a particularly simple case. For very small Debye lengths, shielding of the squeeze potential effectively separates the trapped and passing particles radially. In this regime, the plasma may be described by a simplified model in which trapped and passing particles are divided by a separatrix radius, R_s . The trapped and passing particle densities can be written as $n_t(r) = n_0(r)\Theta(r - R_s)$ and $n_p(r) = n_0(r)\Theta(R_s - r)$, where $\Theta(x)$ is the Heaviside step function. For a top hat density profile, $n_0(r) = n_0\Theta(R_p - r)$, an analytic solution of Eq. (27) is possible.

The potential perturbation is composed of separate solutions in three regions. In region I ($r < R_s$), the mode potential satisfies the Debye shielding equation

$$\frac{1}{r} \frac{\partial}{\partial r} \left(r \frac{\partial}{\partial r} \delta\phi_\ell^I \right) - \frac{\ell^2}{r^2} \delta\phi_\ell^I - \frac{1}{\lambda_D^2} \delta\phi_\ell^I = 0, \quad (28)$$

where $\lambda_D^2 = T/4\pi e^2 n_0$. Since the potential cannot diverge at the origin, we obtain $\delta\phi_\ell^I(r) = I_\ell(r/\lambda_D)$, where I_ℓ is a modified Bessel function of the first kind. In regions II ($R_s < r < R_p$) and III ($r > R_p$), the mode potential satisfies the Laplace equation

$$\frac{1}{r} \frac{\partial}{\partial r} \left(r \frac{\partial}{\partial r} \delta\phi_\ell \right) - \frac{\ell^2}{r^2} \delta\phi_\ell = 0, \quad (29)$$

so we find $\delta\phi_\ell^{II}(r) = A_\ell r^\ell + B_\ell r^{-\ell}$ and $\delta\phi_\ell^{III}(r) = C_\ell (r^\ell - R_w^{2\ell}/r^\ell)$, where use has been made of the boundary condition $\delta\phi_\ell^{III}(R_w) = 0$. Equation (27) also must be satisfied at the interfaces $r = R_s$ and $r = R_p$, where $\partial n_t / \partial r$ gives delta function contributions. This requires that the potential be continuous at the interfaces, $\delta\phi_\ell^I(R_s) = \delta\phi_\ell^{II}(R_s)$ and $\delta\phi_\ell^{II}(R_p) = \delta\phi_\ell^{III}(R_p)$, and that the derivatives satisfy the jump conditions

$$r \frac{\partial}{\partial r} \delta\phi_\ell \Big|_{R_s^+} = \frac{2\ell}{\omega^*} \delta\phi_\ell(R_s) \quad (30)$$

and

$$r \frac{\partial}{\partial r} \delta\phi_\ell \Big|_{R_p^-} = -\frac{2\ell}{\omega^*} \delta\phi_\ell(R_p), \quad (31)$$

where $\omega^* = \ell - \omega/\omega_E$. Eliminating the unknown coefficients A, B, C yields the dispersion relation

$$\left(\frac{R_p}{R_s} \right)^\ell \left(\frac{I_\ell}{\omega^*} + \frac{R_s I_{\ell-1}}{2\ell \lambda_D} \right) \left(\frac{R_w^{2\ell}}{R_p^{2\ell} - R_w^{2\ell}} + \frac{1}{\omega^*} \right) - \left(\frac{R_s}{R_p} \right)^\ell \left(\frac{I_\ell}{\omega^*} + \frac{R_s I_{\ell+1}}{2\ell \lambda_D} \right) \left(\frac{R_p^{2\ell}}{R_p^{2\ell} - R_w^{2\ell}} + \frac{1}{\omega^*} \right) = 0, \quad (32)$$

where $I_\ell \equiv I_\ell(R_s/\lambda_D)$.

There are two roots for Eq. (32) with one above and one below the rotation frequency. The fast mode has a frequency very near the rotation frequency of the column and has not yet been observed in the experiments. For appreciable squeeze voltage, the lower root lies well below the column rotation frequency and corresponds to the experimentally observed mode. The existence of two modes is due to the positive and negative slope of the trapped density profile. This situation is analogous to the inner and outer diocotron modes that exist for hollow profiles.⁷ In the trapped-particle case, the inner (faster) mode is not unstable, since the rotation frequency is monotonically decreasing.

As $\lambda_D \rightarrow 0$, the dispersion relation reduces to

$$\omega^* = \frac{R_w^{2\ell} - R_p^{2\ell}}{R_w^{2\ell} - R_s^{2\ell}} \frac{R_p^{2\ell} - R_s^{2\ell}}{R_p^{2\ell}}. \quad (33)$$

This is the low frequency mode. The high frequency mode has vanished. In this limit, the passing particles behave like a conducting cylinder of radius R_s . This suggests that trapped-particle diocotron modes may exist in a trap with a central conducting cylinder containing two plasma columns that are completely separated axially by a strong squeeze. In that case, the damping mechanism discussed in Sec. V would be absent. Equation (33) provides some quick insight into the qualitative behavior of the low frequency trapped-particle diocotron mode. For low squeeze potentials, R_s approaches the plasma radius and the azimuthal phase velocity of the wave approaches the rotation frequency of the column. At the opposite extreme, the separatrix radius approaches zero and the frequency becomes that of the usual diocotron mode,

$$\omega = \omega_E \left[\ell - 1 + \left(\frac{R_p}{R_w} \right)^{2\ell} \right]. \quad (34)$$

This result is expected since the column has been completely divided and the two halves are effectively decoupled in our reduced description that ignores space charge interactions of the two columns. As we will see, this frequency dependence on squeeze voltage is observed experimentally.

For a careful comparison to experiment, we use the shooting method to obtain a numerical solution of Eq. (27) for realistic density profiles. Input to the theory are the magnetic field strength, voltages on the end rings and barrier electrode, z -integrated density $N(r)$, and temperature $T \equiv T(r=0)$. From these quantities, the equilibrium trapped particle density $n_t(r)$, and separatrix velocity $v_s(r)$ are determined, as discussed in Sec. II, and Eq. (27) is then solved

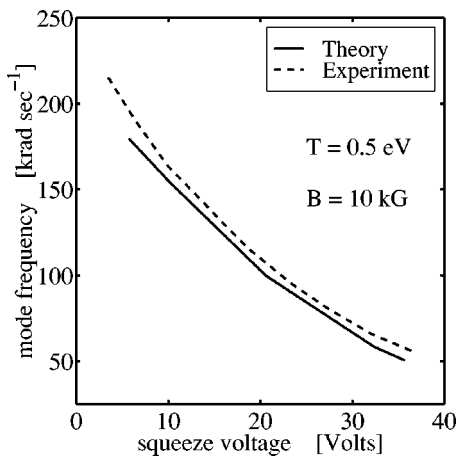


FIG. 5. Mode frequency versus applied squeeze voltage for the low frequency $\ell = 1$ trapped-particle mode. The value varies smoothly between the rotation frequency at the radial edge of the plasma and the usual diocotron mode frequency (i.e., the **EXB** drift frequency at the wall radius).

to find ω . Figure 5 shows a comparison of the calculated and measured mode frequency as a function of squeeze voltage for the temperature $T(r=0)=0.5$ eV and magnetic field $B = 10$ kG. The azimuthal mode number is $\ell = 1$. The agreement is very good (10%), with both curves following the trend expected from the analytic solution. From Eq. (27), one can see trivially that the mode frequency is predicted to scale with magnetic field strength as $\omega \propto 1/B$. This scaling is observed experimentally to an accuracy of 2% over the range 300 G to 10 kG.⁸ Although the temperature enters Eq. (27) explicitly and implicitly [e.g., through $n_t(r)$, $n_p(r)$ and $v_s(r)$] the solutions for ω exhibit only a weak dependence on temperature, changing less than 5% as the temperature is varied by an order of magnitude. Measurements also show only a weak dependence; ω varies by 5% as T varies over 0.5–5.0 eV.

The density perturbation of the trapped-particle mode vanishes at a specific radius. Inside this radius, the majority of particles involved in the oscillation are passing and move adiabatically along field lines. Outside this radius, the particles are mostly trapped and experience drift motion. Experimental and calculated density eigenfunctions at low and high squeeze voltages are shown in Fig. 6. The zero crossing of the density perturbation decreases as the squeeze voltage is increased. This is expected since the stronger barrier traps more particles.

There is qualitative agreement but small systematic discrepancy in the measured and observed eigenfunctions. At low squeeze voltage, the theoretical model predicts a smaller passing particle perturbation than is observed in the experiment. At high squeeze voltage, the model predicts a larger perturbation in the passing particles than is observed. The origin of this discrepancy remains unclear. The discrepancy in δn for $r > 1.5$ cm is due to a truncation of the density profile. The experimentally measured density profiles exhibit a small tail out at large radii. It is unknown whether this tail is real or some artifact of the measurement process. To avoid singularities in Eq. (27) caused by a wave-fluid resonance, we have smoothly truncated the experimentally measured

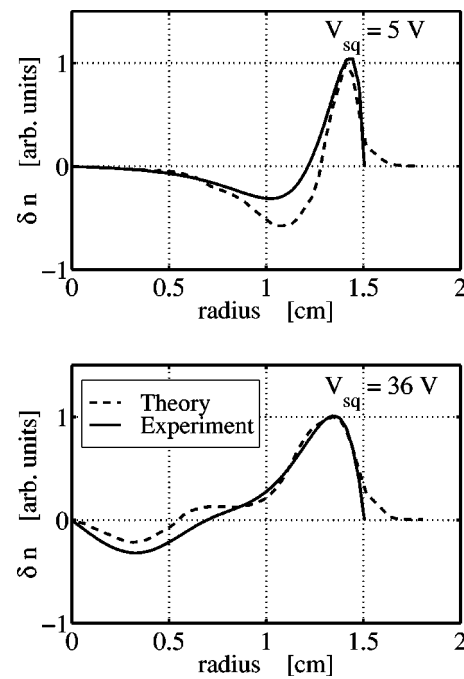


FIG. 6. Experimental and theoretical density eigenfunctions for the low frequency trapped-particle mode at -5 and -36 Volt squeeze. The theoretical calculation used a density profile that was truncated at 1.5 cm. At outer radii the trapped particles produce a positive perturbation. At inner radii the shielding response of the passing particles gives a negative perturbation. The radius of the zero crossing becomes smaller as the barrier strength is increased.

density profile (at $r = 1.5$ cm) for use in the calculation. The experimental eigenfunction also contains a nonzero imaginary part. However, Fig. 6 compares the real parts of the eigenfunctions. In the collisionless theory, δn is purely real.

The mode potentials for plasmas at various temperatures (0.1, 0.5, 1.0, 5.0 eV) are shown in Fig. 7. The Debye shielding phenomenon resulting from the adiabatic motion of the passing particles is readily observed. As the temperature is decreased, the potential created by the trapped particle den-

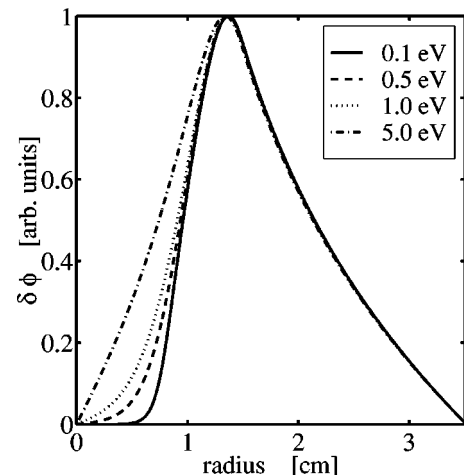


FIG. 7. Mode potentials $\delta\phi_1(r)$ at various temperatures. The Debye shielding phenomenon resulting from the adiabatic motion of the passing particles is apparent. At low temperature, the mode potential is excluded from the interior of the column where the majority of particles are passing.

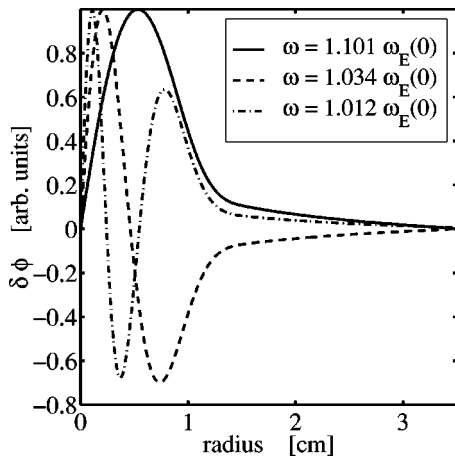


FIG. 8. Theory predicts additional eigenmodes with frequencies above the peak rotation frequency of the column [$\omega_E(0)$]. The mode potentials for three such eigenmodes are shown. These high frequency modes are highly self-shielded (i.e., significant potentials do not exist in the vacuum region outside the plasma column).

sity perturbation remains essentially unchanged. However, the passing particles shield this potential from the interior of the column at very low temperatures.

As mentioned earlier, Eq. (32) predicts the existence of another trapped-particle mode that has an azimuthal phase velocity above the column rotation frequency. With this in mind, we return to the full kinetic model and look for numerical solutions of Eq. (27) for $\omega > \ell \omega_E(0)$. In fact, we have found several eigenmodes in this high frequency range. Figure 8 shows plots of eigenmode potentials for three such trapped-particle modes. In this case, the plasma was characterized by the density profiles in Fig. 4, a magnetic field of 10 kG, and a temperature of 1 eV. The potential perturbations are indexed by the number of radial nodes, n_r . As the radial nodes increase the azimuthal phase velocity of the waves asymptotes to the rotation frequency at the axis [$\omega_E(r=0)$]. For $n_r=0$, the phase velocity is 10% above the peak plasma rotation frequency and the electric field at the trap wall is 0.44% that of the lower branch mode. A small radial electric field at the wall is a feature common to all of the high frequency modes. This makes them extremely difficult to observe experimentally. Typically, diocotron modes are launched and detected by applying time varying voltages to the wall sectors. The coupling of these self-shielded modes to the wall sectors is very weak. However, if the modes are excited by some other means, the density eigenfunctions can be observed by dumping the plasma.

In Fig. 9, the trapped and passing density perturbations are shown for the low frequency and $n_r=1$ high frequency modes. For the low frequency mode, the main perturbation of trapped particles occurs at outer radii, and the passing perturbation is at inner radii. In this situation, the potential is effectively shielded from the column interior. In the high frequency oscillation, the main trapped and passing particle perturbations occur at inner radii. However, the trapped-particle perturbation is larger and a substantial mode potential exists at inner radii (see Fig. 8).

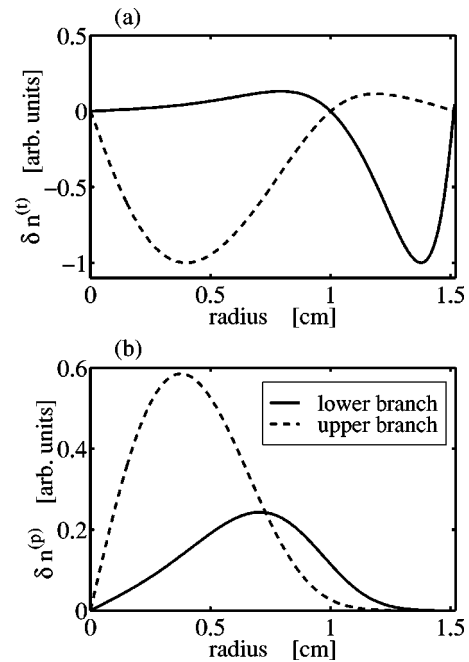


FIG. 9. Trapped (a) and passing (b) density perturbations for the low frequency and first high frequency modes. For the lower branch, trapped and passing density perturbations are well-separated radially. For the upper branch, both trapped and passing perturbations occur at inner radii.

V. COLLISIONS

In this section, we return to the discussion of the low frequency trapped-particle diocotron mode and investigate the effects of collisions between particles. Because the trapped particles and the passing particles experience different dynamics, the mode perturbation in the velocity distribution is discontinuous in collisionless theory. Setting $\langle \delta\phi_\ell \rangle = 0$ in Eqs. (18) and (19) yields

$$\delta f_{\ell j}(r,v) = \begin{cases} \frac{e \delta\phi_{\ell j}}{T} f_0(r,v), & |v| > v_s(r), \\ \frac{c\ell}{Br} \frac{\delta\phi_{\ell j}}{\omega'} \frac{\partial f_0(r,v)}{\partial r}, & |v| < v_s(r), \end{cases} \quad (35)$$

where we have used $f^{(v)}(r,v) = f_0(r,v)$ for $|v| < v_s(r)$ and $f^{(p)}(r,v) = f_0(r,v)$ for $|v| > v_s(r)$. This expression for $\delta f_{\ell j}(r,v)$ is discontinuous in value and slope at $v = v_s(r)$. When collisions are added to the theory, the Fokker-Planck collision operator contains velocity derivatives that become arbitrarily large at such a discontinuity, so the effect of collisions on $\delta f_{\ell j}$ cannot be ignored, even if ν is small. Small angle scattering provides an essential correction, smoothing the distribution in a boundary layer near the separatrix. In Fig. 10, the perturbed distribution function at a specific radius is plotted versus velocity. The solid line represents $\delta f_{\ell j}$ from collisionless theory and clearly depicts the discontinuity at the separatrix velocity. The dashed line is the real part of the collisional correction to $\delta f_{\ell j}$ which removes the discontinuity. We will derive this correction shortly. Significantly, the correction contains an imaginary component (dotted-dashed line) that is in phase with the mode electric field, so the mode can exchange energy with the scattered

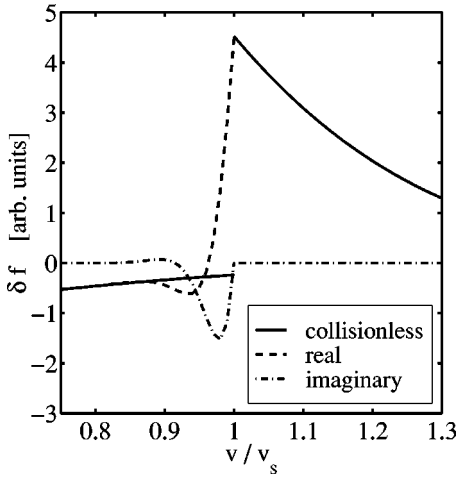


FIG. 10. Perturbed distribution function at $r=1$ cm. The solid line represents collisionless theory and exhibits a discontinuity at the separatrix radius. The dashed lines contain the corrections to the real and imaginary parts of δf due to collisional diffusion. In this case, collisions have smoothed out the discontinuity over a width $\delta v \approx 0.1v_s$.

particles and damp as a consequence. We will show that the velocity scattering and damping are intrinsically associated with a kind of neo-classical radial transport.

Including the effect of collisions, the trapped-particle perturbation satisfies the equation

$$\left\{ i\omega' - D_v(v_s) \frac{\partial^2}{\partial v^2} \right\} \delta f_\ell^{(t)} = \frac{ic\ell}{Br} \delta\phi_\ell \frac{\partial f_0}{\partial r}, \quad (36)$$

where only the second derivative term in the Fokker-Planck collision operator has been retained. In the separatrix boundary layer region, where derivatives are large, the second velocity derivative term suffices. Here, $D_v(v_s)$ is the coefficient of parallel velocity diffusion evaluated at the separatrix velocity $v_s = v_s(r)$ and is given by Eq. (10).

For $\ell > 0$, the solution to Eq. (36) is given by

$$\delta f_\ell^{(t)} = \frac{c\ell}{Br} \frac{\delta\phi_\ell}{\omega'} \frac{\partial f_0}{\partial r} + a \exp \left[\frac{1+i}{\sqrt{2}} \sqrt{\frac{\omega'}{D_v(v_s)}} (v - v_s) \right], \quad (37)$$

where a is an arbitrary constant and we have chosen the sign so that the exponential decays as $(v - v_s)$ becomes large and negative. The new term represents a collisional correction in a boundary layer of width $\delta v_s^{(t)} \sim \sqrt{D_v(v_s)/\omega'}$. To understand this width, note that the sign of the perturbation seen by the trapped particles changes on the time scale $1/\omega'$, and velocity diffusion can extend to the width $\delta v_s^{(t)}$ during this time [i.e., $(\delta v_s^{(t)})^2 \sim D_v(v_s)/\omega'$].

Similarly, the passing-particle perturbation satisfies the equation

$$\left\{ v \frac{\partial}{\partial z} + \frac{e}{m} \frac{\partial \phi_0}{\partial z} \frac{\partial}{\partial v} - D_v(v_s) \frac{\partial^2}{\partial v^2} \right\} \left(\delta f_\ell^{(p)} - \frac{e\delta\phi_\ell}{T} f_0 \right) = 0, \quad (38)$$

where we have used $C(f_0) = 0$. The solution of Eq. (38) requires some information concerning the z -dependence of the

mode quantities, but we can obtain an order of magnitude estimate to the collisional correction to $\delta f_\ell^{(p)}$ by noting that the operator,

$$v \frac{\partial}{\partial z} + \frac{e}{m} \frac{\partial \phi_0}{\partial z} \frac{\partial}{\partial v} \approx i\omega_b, \quad (39)$$

is a derivative along a bounce orbit, which can be taken of order ω_b since passing particles see the mode quantities change by order unity during a bounce orbit. Substituting Eq. (39) into Eq. (38) and solving the resulting equation yields

$$\delta f_\ell^{(p)} = \frac{e\delta\phi_\ell}{T} f_0 + b \exp \left[\frac{-(1+i)}{\sqrt{2}} \sqrt{\frac{\omega_b}{D_v(v_s)}} (v - v_s) \right]. \quad (40)$$

In this case, the correction is of width $\delta v_s^{(p)} \sim \sqrt{D_v(v_s)/\omega_b}$, since the passing particles see a sign change on the bounce time scale $1/\omega_b$.

There is a disparity between the width of the boundary layer for trapped and passing particles: $\delta v_s^{(p)} \ll \delta v_s^{(t)}$ since $\omega_b \gg \omega'$. The consequence of this disparity is that only the trapped-particle correction contributes significantly to the damping. Choosing a and b so that the value and slope of the distribution are continuous at $v = v_s$ yields

$$a = \delta\phi_\ell \left[\frac{ef_0}{T} - \frac{c\ell}{Br\omega'} \frac{\partial f_0}{\partial r} \right]_{v=v_s} \left(\frac{\sqrt{\omega_b}}{\sqrt{\omega_b} + \sqrt{\omega'}} - \frac{\sqrt{2}}{1+i} \frac{\sqrt{D_v}}{\sqrt{\omega_b} + \sqrt{\omega'}} \frac{mv_s}{T} \right), \quad (41)$$

and

$$b = -\delta\phi_\ell \left[\frac{ef_0}{T} - \frac{c\ell}{Br\omega'} \frac{\partial f_0}{\partial r} \right]_{v=v_s} \left(\frac{\sqrt{\omega'}}{\sqrt{\omega_b} + \sqrt{\omega'}} + \frac{\sqrt{2}}{1+i} \frac{\sqrt{D_v}}{\sqrt{\omega_b} + \sqrt{\omega'}} \frac{mv_s}{T} \right). \quad (42)$$

Dropping terms of order $\sqrt{\omega'/\omega_b}$ gives $a = \delta\phi_\ell [ef_0/T - (c\ell/Br\omega')(\partial f_0/\partial r)]_{v=v_s}$ and $b = 0$. Substituting into Poisson's equation then yields an eigenvalue equation for the mode potential,

$$\nabla_\perp^2 \delta\phi_\ell = 4\pi e \left\{ \frac{en_p}{T} + \frac{c\ell}{Br} \frac{\partial n_t}{\partial r} \frac{1}{\omega'} + \frac{2\sqrt{2}}{1+i} \sqrt{\frac{D_v(v_s)}{\omega'}} \left[\frac{ef_0}{T} - \frac{c\ell}{Br} \frac{\partial f_0}{\partial r} \frac{1}{\omega'} \right]_{v=v_s} \right\} \delta\phi_\ell, \quad (43)$$

which is subject to the boundary conditions $\delta\phi_\ell(0) = \delta\phi_\ell(R_w) = 0$. Multiplying both sides of Eq. (43) by $\delta\phi_\ell^*$, integrating over rdr , setting $\omega = \omega_r + i\gamma$, and taking the imaginary part of both sides yields an expression for the growth or damping rate,

$$\gamma = \frac{\frac{B}{c\ell} \int_0^{R_w} r dr |\delta\phi_\ell|^2 \sqrt{\frac{2D_v(v_s)}{\ell\omega_E - \omega_r}} \left[\frac{ef_0}{T} - \frac{c\ell}{Br} \frac{df_0}{dr} \frac{1}{\ell\omega_E - \omega_r} \right]_{v=v_s}}{\int_0^{R_w} dr \frac{|\delta\phi_\ell|^2}{(\ell\omega_E - \omega_r)^2} \frac{\partial n_t}{\partial r}}. \quad (44)$$

For the plasmas considered here, the numerator in Eq. (44) is positive and the denominator is negative so that the mode is damped. To lowest order in the small parameters γ/ω_r and $\sqrt{\nu/(\ell\omega_E - \omega_r)}$, the eigenmode $|\delta\phi_\ell|$ may be approximated by the eigenmode for $\nu=0$. Indeed, the γ values predicted in this way by Eq. (44) agree closely with those obtained by direct numerical solution of Eq. (43) using a shooting method.

To understand the energy budget for the damping, we rewrite Eq. (44) as

$$\begin{aligned} 0 &= 2\gamma W \\ &+ \int_0^{R_w} r dr \int_0^{2\pi} d\theta 2e\delta\phi(r, \theta, t) \frac{d}{dt} [L\delta n_c(r, \theta, t)] \\ &+ \int_0^{R_w} r dr \int_0^{2\pi} d\theta \left[-e \frac{\partial\phi_0}{\partial r} \right] \\ &\times [\delta v_r(r, \theta, t) \delta n_c(r, \theta, t) 2L], \end{aligned} \quad (45)$$

where

$$W = \frac{2Le c \omega \ell}{B} \int_0^{R_w} 2\pi dr \frac{|\delta\phi_\ell|^2}{(\ell\omega_E - \omega_r)^2} \frac{\partial n_t}{\partial r} \quad (46)$$

is the mode energy, which turns out to be negative. The first term in Eq. (45) is the rate of change of mode energy, which is positive during damping since both W and γ are negative. In the second term, the quantity $\delta n_c(r, \theta, t)$ is the collisional correction to the trapped electron perturbation, and the convective derivative $d(L\delta n_c)/dt = (\partial/\partial t + \omega_E \partial/\partial \theta)(\delta n_c L)$ is the flux of scattered electrons to the side where the mode potential is $+\delta\phi(r, \theta, t)$. As an electron moves along the magnetic field lines from the side where the potential is $-\delta\phi$ to the side where it is $+\delta\phi$, the mode does work $2e\delta\phi$ on the electron. The second term is the rate of such work, which turns out to be positive. In the third term, the quantity $\delta v_r(r, \theta, t) = -(c/Br)(\partial\delta\phi/\partial\theta)$ is the radial drift velocity imparted by the mode potential, so the product $(\delta v_r \delta n_c)$ is the radial flux of scattered particles. Thus, the third term is the rate at which the mode does work in moving the scattered particles through the potential gradient $\partial\phi_0/\partial r$. There is a net outward radial flux of scattered particles, so the third term is negative, balancing the other two terms. In summary, the mode potential increases the kinetic energy of the scattered particles by acceleration along the magnetic field and decreases the electrostatic energy of the particles by radial transport outward, the latter effect being dominant. When the liberated energy is added to the negative energy mode, the mode damps.

To understand the sign of the second term, first recall that in the absence of collisions, $\delta f_p(v_s) > 0$ and $\delta f_i(v_s)$

< 0 on the side where $\delta\phi > 0$. On this side, the smoothing action of collisions must produce a velocity-space flux from passing to trapped. The situation is reversed on the other side where $\delta\phi < 0$. Thus, the net effect is a spatial flux of trapped particles from the side where $\delta\phi < 0$ to the side where $\delta\phi > 0$. Physically, this is reasonable, since we expect collisions to produce a flux of trapped particles from the high potential energy side ($-e\delta\phi > 0$) to the low potential energy side ($-e\delta\phi < 0$). Equivalently, we expect collisions to produce heating, and the second term is the heating rate.

The θ -average radial flux is given by

$$\frac{1}{2\pi} \int_0^{2\pi} d\theta \delta v_r \delta n_c = D_r(r) \left[-\frac{\partial n_0}{\partial r} + \frac{e}{T} \frac{\partial\phi'_0}{\partial r} n_0 \right], \quad (47)$$

where $D_r(r) = \epsilon(\Delta r)^2 \omega'$ is a neo-classical like diffusion coefficient. To understand this coefficient, note first that $\epsilon = 2\sqrt{2D_v(v_s)}/\omega' \exp[-v_s^2/2\bar{v}^2]/\sqrt{2\pi\bar{v}^2}$ is the fraction of particles in the boundary layer at radius r , where $v_s = v_s(r)$. In the absence of the mode, the $\mathbf{E} \times \mathbf{B}$ drift orbits are circular for all of the particles. In the presence of the mode, the orbits for the trapped particles are distorted from circularity by an amount $\Delta r = c\ell|\delta\phi_\ell|/Br\omega'$, and the distortions on the two ends are 180° out of phase. When a trapped particle is scattered and changes trapped-particle class (and drift orbit), the particle effectively makes a radial step Δr . For the particles in the boundary layer, the class changes at the rate ω' .

Equation (47) is the usual form for the transport flux in the presence of a density gradient and an external force with the diffusion and mobility coefficients related by an Einstein relation⁹ [i.e., $\mu = (e/T)D$]. The radial electric field $-\partial\phi'_0/\partial r = -\partial\phi_0/\partial r + (r\omega_\ell/\ell)(B/c)$ is the effective field in the rotating frame of the wave. This is the frame where the mode perturbation is static and the Einstein relation is valid. One can easily understand that diffusion in a negative density gradient ($\partial n_0/\partial r < 0$) produces an outward radial flux. However, the origin of the mobility term is more subtle. In $\mathbf{E} \times \mathbf{B}$ drift motion, electrons can move radially only due to an azimuthal electric field. Why then is there a preference for transport in the direction of the radial electric force?

In fact, this radial mobility preference is intimately connected with the net axial flux of scattered particles from the high potential energy side ($-e\delta\phi > 0$) to the low potential energy side ($-e\delta\phi < 0$). The preference for outward radial transport when $e\partial\phi'_0/\partial r > 0$ is illustrated by the schematic diagram in Fig. 11. For the case $\ell = 1$, the solid curves represent potential energy contours [i.e., $-e\phi'_0(r) - e\delta\phi(r, \theta) = \text{const}$] on one side of the barrier, and the dashed curves the contours on the other side. The difference between the two arises from the fact that $\delta\phi$ has opposite signs in the two

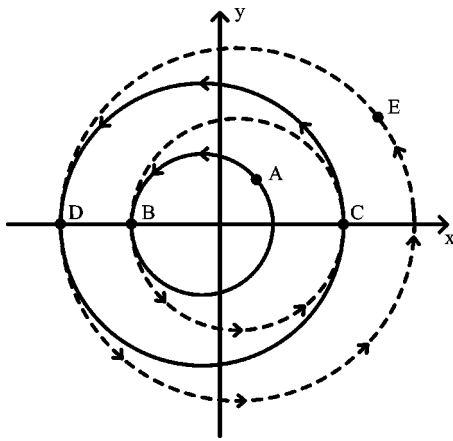


FIG. 11. Potential energy contours in the rotating frame of an $\ell=1$ wave (solid $z>0$, dashed $z<0$). A particle initially at point A is transported to point E through orbits along potential contours and detrapping/retrapping collisions at points B, C and D. For azimuthal phase velocity less than the column rotation frequency, marginally trapped particles are more likely to be scattered through the squeeze region when farthest from the trap center and thus are transported radially outward.

ends. If we work in the rotating frame of the wave, the pattern is stationary (except for the slow damping). A particle that is initially trapped in one end at point A will $\mathbf{E} \times \mathbf{B}$ drift along the contours until it comes to the point B where the contour is farthest from the center; that is, where $-e\delta\phi(r, \theta)$ takes its maximum value. Statistically, this is the point where the particle is most likely to be detrapped and move rapidly to the other end, where this particle or an equivalent particle is scattered and trapped. The particle will then $\mathbf{E} \times \mathbf{B}$ drift along the dashed contour, continuing its motion outward to point C. Repeating the process then takes the particle to points D and E.

If the sign of $e\partial\phi'_0/\partial r$ changes to negative, the dashed curves change into solid curves and *vice versa*, but this relabeling is not significant. The important change is that the particle now $\mathbf{E} \times \mathbf{B}$ drifts azimuthally in the opposite sense, and so spirals radially inward ($E \rightarrow D \rightarrow C \rightarrow B \rightarrow A$). The jumps from one side to the other now happen when the contour is closest to the center.

The sign of $e\partial\phi'_0/\partial r$ changes to negative if the angular velocity of the rotating frame exceeds the plasma rotation velocity. This implies that rapidly rotating asymmetric potentials can be used to compress the plasma radially. This technique has been known for some time and is generally known as the “rotating wall” effect.¹⁰ We suggest that trapped-particle transport is the microscopic mechanism of the “rotating wall” in some circumstances.

Another frame in which $e\partial\phi'_0/\partial r$ is negative is one that co-rotates with a high frequency trapped-particle mode. An analysis similar to that given above for the low frequency mode reveals that the high frequency modes are also damped by the same collisional scattering process. The high frequency modes are self-shielded with the potential perturbation being largest at inner radii where $\partial n_i/\partial r$ is positive. As a result, the wave energy given by integral (46) is positive for the high frequency modes. Again, energy conservation requires that the third term of Eq. (45) cancel the first two

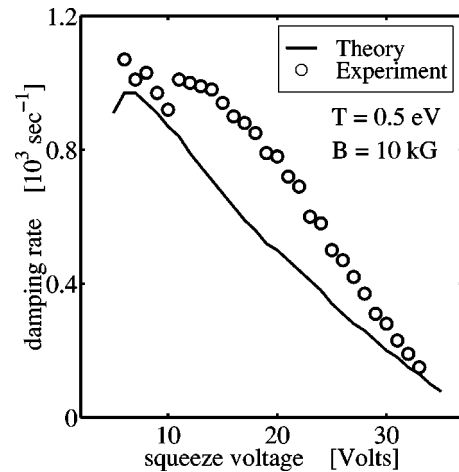


FIG. 12. Mode damping rate vs applied squeeze voltage from theory [Eq. (44)] and experiments.

terms. The second term represents the work done by the wave as particles move axially and remains $2e\delta\phi$. Since the first two terms now have opposite signs, the third term could be either positive or negative. However, for the high frequency modes $(\omega_r - \ell\omega_E)^2$ is usually quite small and the first term is large and positive. This requires the third term to be negative. Therefore, the damping of the high frequency modes is associated with a net inward radial flux. Flux can be inward because $\partial\phi'_0/\partial r$ is negative for high frequency modes.

Finally, we compare the measured and predicted and damping rates for the lower frequency mode using realistic density profiles in the theory. Figures 12, 13 and 14 show a comparison of the predicted and measured rates versus squeeze voltage, magnetic field strength, and temperature, respectively. The agreement is to within 50% over the expected range of validity for the theory. To understand the scaling trends we turn to Eq. (44). Since the denominator increases with the number of trapped particles, which increases with the squeeze voltage, the damping rate is ex-

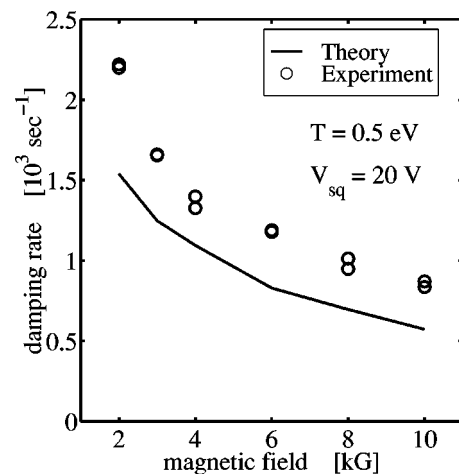


FIG. 13. Mode damping rate vs magnetic field. The theory correctly predicts the $B^{-1/2}$ at high magnetic fields. At low field, the fast bounce assumption is violated and the theory breaks down.

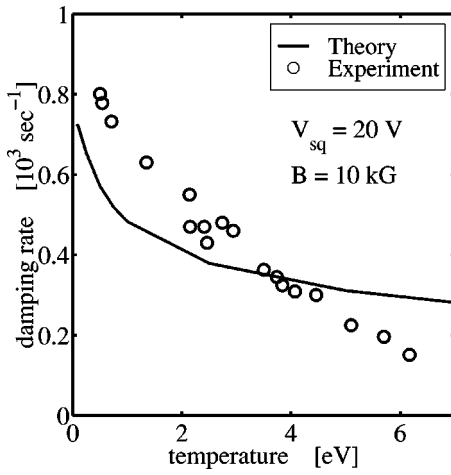


FIG. 14. Mode damping rate vs temperature.

pected to be a decreasing function of the squeeze voltage, and this trend is apparent in Fig. 12. Since ω_r and ω_E are proportional to $1/B$, Eq. (44) implies that γ scales as $1/\sqrt{B}$. This scaling is observed for large field strength ($B \approx 2 - 10$ kG), where the theory assumption $\omega_b \gg \omega_E, \omega_r$ is well satisfied, but $\gamma \propto 1/B$ scaling is observed at a lower field strength. This latter scaling is not understood theoretically.

Figure 14 shows that the measured and calculated damping rates are decreasing functions of temperature over the range of measurements ($T = 0.5 - 6$ eV), with the experiments showing a somewhat stronger temperature dependence. The discrepancy may be due to a radial dependence in the plasma temperature. There are some experimental indi-

cations that heating from radial transport caused by ambient field errors raises the temperature more at large r , where the damping mechanism acts, than at $r = 0$, where the temperature is measured. Moreover, the temperature inhomogeneity is more pronounced at higher temperatures where the cross-field heat conduction is lower. Including such a correction to the plasma temperature changes the slope of the measured values toward agreement with the theory.

Recent experiments have demonstrated a correspondence between the damping of trapped-particle diocotron modes and asymmetry-induced transport.¹¹ In these experiments, trapped particles are created in the usual manner with an applied “squeeze” voltage. Static field errors (such as magnetic tilt) are introduced in the trap and produce perturbed drift orbits that are quantitatively similar to drift orbits associated with trapped-particle modes. The rate of radial expansion of the plasma column is found to be proportional to the damping rate of the trapped-particle diocotron mode over a wide range of plasma parameters. This correspondence strongly suggests velocity space diffusion of marginally trapped particles as the microscopic mechanism responsible for asymmetry-induced transport.

VI. LANDAU RESONANCES

Wave-particle resonances are possible for this mode, but the associated Landau damping is small compared to the collisional damping provided $\bar{\omega}_b \gg |\ell \omega_E(r) - \omega_r|$. Here, $\bar{\omega}_b$ is the axial bounce frequency for a thermal particle. In Appendix A, we neglect collisional damping and obtain the following expression for the Landau damping rate:

$$\gamma_{LD} = - \frac{\pi \int_0^{R_w} r dr \int_0^\infty dI \sum_{n \neq 0} \left[\ell \frac{\partial f_0}{\partial p_\theta} - n \omega_b \frac{f_0}{T} \right] |\delta H_{\ell, n}|^2 \delta[n \omega_b + \ell \omega_E - \omega_r]}{\int_0^{R_w} r dr \int_0^\infty dI \frac{\ell \frac{\partial f_0}{\partial p_\theta} |\delta H_{\ell, 0}|^2}{(\ell \omega_E - \omega_r)^2}}, \quad (48)$$

where $|\ell \omega_E - \omega_r|/\bar{\omega}_b$ and $\gamma_{LD}/|\ell \omega_E - \omega_r|$ are assumed to be small. Equation (48) employs the canonical variables $(\theta, p_\theta, I, \psi)$, where $p_\theta = -eBr^2/2c$ is the canonical angular momentum conjugate to θ , and (I, ψ) are action-angle variables defined for the equilibrium Hamiltonian,

$$H_0 = \frac{p_z^2}{2m} - e\phi_0(p_\theta, z). \quad (49)$$

The action is defined in the usual manner,

$$I(p_\theta, H_0) = \frac{1}{2\pi} \oint dz' p_z[z', H_0, p_\theta], \quad (50)$$

and the Hamiltonian $H_0 = H_0(I, p_\theta)$ is obtained by inversion. The rotation and bounce frequencies are then given by

$$\omega_E(I, p_\theta) = \frac{\partial H_0}{\partial p_\theta}, \quad \omega_b(I, p_\theta) = \frac{\partial H_0}{\partial I}. \quad (51)$$

The angle variable is given by

$$\psi = \sqrt{\frac{m}{2}} \int^z \frac{dz' \frac{\partial H_0}{\partial I}}{\sqrt{H_0(I, p_\theta) + e\phi_0(p_\theta, z')}}, \quad (52)$$

and the bounce harmonic of the mode potential by

$$\delta H_{\ell, n} = \frac{1}{2\pi} \int_0^{2\pi} d\psi e^{-in\psi} (-e) \delta\phi_\ell[z(\psi, p_\theta, I), p_\theta]. \quad (53)$$

With these definitions and expression (48), one can understand the issue that determines whether or not Landau

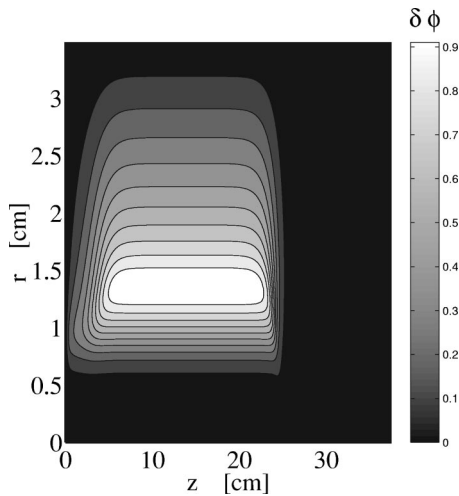


FIG. 15. Contour plot of mode potential showing axial dependence in the squeeze region and near the column end. Since the axial bounce frequency is large as compared to the mode frequency, Debye shielding forces the mode potential to be z -independent in the main part of the column. For $B = 4$ kG a resonant particle at $r = 1.2$ cm the turning points are 6.8 and 21.2 cm and the resonant energy exchange is small.

damping is negligible. By hypothesis, the bounce frequency for a thermal particle, $\bar{\omega}_b = \omega_b(\bar{I}, p_\theta)$, is large compared to the Doppler shifted mode frequency $|\ell\omega_E - \omega|$.

Consequently, the argument of the delta function in Eq. (48) can vanish only for two special classes of particles. The first class consists of particles that are very close to the separatrix; the bounce frequency for these particles can be much smaller than $\bar{\omega}_b$. However, direct calculation shows that these particles lie well within the collision dominated boundary layer, provided $\bar{\omega}_b \gg |\ell\omega_E - \omega_r|$, so rapid collisional trapping and de-trapping destroys the Landau resonance. The second class consists of very slow particles (i.e., $I \ll \bar{I}$) that are deeply trapped on one side of the barrier or the other. These particles can provide significant Landau damping only if $\delta H_{\ell,n}(I, p_\theta)$ is substantial for the low values of I required for frequency resonance.

Recall that Debye shielding forces $\delta\phi_\ell(z, r)$ to be nearly z -independent in the trapped particle regions well away from the squeeze barrier. If $\delta\phi_\ell(z, p_\theta)$ were exactly z -independent over the region of z accessible to the deeply trapped particles, then Eq. (53) would imply that $\delta H_{\ell,n} = 0$, and there would be no Landau damping. Thus, the strength of the Landau damping depends on the degree of z -dependence for $\delta\phi_\ell(z, r)$ in the accessible region.

In Appendix B, we obtain approximate numerical solutions for the z -dependence of the mode potential. As an example of the results, Fig. 15 shows the potential contours for the specific case of the density profiles in Fig. 4: a -20 V squeeze voltage, and a temperature of 1 eV. Using this solution for $\delta\phi_1(r, z)$, we evaluate expression (48) and obtain the Landau damping rate. Figure 16 shows a comparison of the Landau and collisional damping rates at several values of magnetic field strength. For $B > 2$ kG, the Landau damping rate is predicted to be negligible and collisions dominate the damping. In this high magnetic field regime the mode frequency is small compared to the bounce frequency. There-

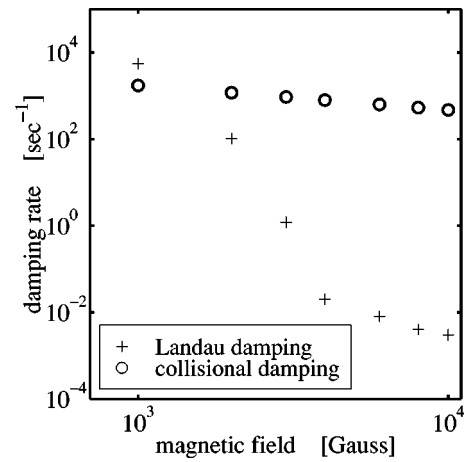


FIG. 16. Mode damping rate due to Landau resonance and collisions versus magnetic field. At high fields, particles that bounce in resonance with the wave oscillation are very deeply trapped and do not experience significant axial electric fields of the mode. As a result, collisions dominate the damping process.

fore, only very deeply trapped particles bounce resonant with the wave and the wave-particle energy exchange is small. As the magnetic field strength is reduced, the mode frequency increases while the axial bounce frequency of the particles remains fixed. For low enough values of B , weakly trapped and even passing particles come into bounce resonance with the wave and the wave-particle energy exchange is larger. Near $B = 1$ kG, the Landau damping rate is predicted to exceed the collisional rate. However, in this low magnetic field regime $\bar{\omega}_b \approx |\omega_E - \omega_r|$, so a basic assumption of our theory is violated.

VII. CONCLUSION

We have developed a quasi-3D model for the newly discovered trapped-particle diocotron mode. The mode consists of two diocotron oscillations that are excited 180° out of phase on either side of an applied squeeze barrier. The mode dynamics consists of trapped particles executing $\mathbf{E} \times \mathbf{B}$ drift motion, while passing particles stream along field lines in a Debye shielding action. The model developed here accurately predicts the frequency and eigenmode structure of the experimentally observed mode over a range of plasma parameters. Furthermore, the model predicts the existence of additional trapped-particle modes that have azimuthal phase velocities above the maximum column rotation frequency.

We have also identified the damping mechanism of the trapped-particle diocotron modes as velocity diffusion in a boundary layer near the trapped-passing separatrix. An analysis based on Fokker-Planck collisions yields a damping rate for the mode that agrees with observations to within 50% and predicts the essential scaling with plasma parameters. The damping of the negative energy modes is associated with a net outward radial flux of particles, and the damping of the positive energy modes is associated with a net inward radial flux of particles. Recent experiments suggest that the mechanism responsible for transport in the trapped-particle modes may be responsible as well for trans-

port observed when static field asymmetries are applied to the plasma.¹¹ Finally, the full 3D mode potential was calculated and used to show that Landau damping of the trapped-particle modes is negligible in the high magnetic field limits, but may become the dominant damping process for low fields.

ACKNOWLEDGMENTS

The authors enjoyed useful discussions with A. A. Kambantsev, C. F. Driscoll, J. H. Yu, D. H. E. Dubin, R. Spencer, and G. Mason.

This work was supported by National Science Foundation Grant No. PHY-9876999 and Office of Naval Research Grant No. N00014-96-1-0239.

APPENDIX A: DERIVATION OF LANDAU DAMPING EXPRESSION

Here, we derive an expression for rate of change in the trapped-particle wave amplitude due to interactions with bounce-resonant electrons. Since the trap is axisymmetric and the wall voltages are static, the total energy and canonical angular momentum are conserved quantities. Therefore, the unperturbed Hamiltonian is integrable and it is possible to obtain a canonical transformation to action-angle variables $(\theta, p_\theta, \psi, I)$. This transformation is carried out formally in Ref. 12. In the new coordinates Eq. (5) becomes

$$\left(\frac{\partial}{\partial t} + \frac{\partial H_0}{\partial I} \frac{\partial}{\partial \psi} + \frac{\partial H_0}{\partial p_\theta} \frac{\partial}{\partial \theta} \right) \delta f = \left(\frac{\partial f_0}{\partial I} \frac{\partial}{\partial \psi} + \frac{\partial f_0}{\partial p_\theta} \frac{\partial}{\partial \theta} \right) \delta H, \quad (\text{A1})$$

where $C=0$ in the present collisionless analysis. Here $p_\theta = -eBr^2/2c$ is the radial coordinate, $I = \oint p_z(z, p_\theta, H_0) dz$ is the bounce action and $\delta H = -e \delta \phi$ is the perturbed Hamiltonian. θ and ψ are the variables canonically conjugate to p_θ and I , respectively. We assume that the equilibrium satisfies the Boltzmann condition so that $\partial f_0 / \partial H_0 = -f_0 / T$. Solving Eq. (A1) for perturbations that vary as $\exp[i(n\psi + \ell \omega_E - \omega t)]$ we obtain

$$\delta f_{\ell, n} = \left[\frac{\ell \frac{\partial f_0}{\partial p_\theta} - n \omega_b \frac{f_0}{T}}{n \omega_b + \ell \omega_E - \omega} \right] \delta H_{\ell, n}, \quad (\text{A2})$$

where $\omega_b = \partial H_0 / \partial I$ is the bounce frequency and $\omega_E = \partial H_0 / \partial p_\theta$ is the bounce averaged rotation frequency.

Substituting into the Poisson equation gives

$$\begin{aligned} & \left[\frac{1}{r} \frac{\partial}{\partial r} \left(r \frac{\partial}{\partial r} \right) - \frac{\ell^2}{r^2} + \frac{\partial^2}{\partial z^2} \right] \delta \phi_\ell \\ &= -4\pi e \int_{-\infty}^{+\infty} dv \sum_{n=-\infty}^{+\infty} e^{in\psi} \left[\frac{\ell \frac{\partial f_0}{\partial p_\theta} - n \omega_b \frac{f_0}{T}}{n \omega_b + \ell \omega_E - \omega} \right] \delta H_{\ell, n}. \end{aligned} \quad (\text{A3})$$

Multiplying the term on the left hand side of Eq. (A3) by $\delta \phi_\ell^*$ and integrating over the volume of trap yields a real quantity. Therefore, it must also be true that

$$\begin{aligned} 0 = \text{Im} & \left\{ \int_0^{R_w} 2\pi r dr \int_{-\infty}^{+\infty} dz \int_{-\infty}^{+\infty} dv \sum_{n, n'=-\infty}^{+\infty} e^{i(n-n')\psi} \right. \\ & \left. \times \left[\frac{\ell \frac{\partial f_0}{\partial p_\theta} - n \omega_b \frac{f_0}{T}}{n \omega_b + \ell \omega_E - \omega} \right] \delta H_{\ell, n'}^* \delta H_{\ell, n} \right\}. \end{aligned} \quad (\text{A4})$$

Since phase space volume is conserved in Hamiltonian systems, $mdvdz = dI d\psi$, we can rewrite Eq. (A4) as

$$\begin{aligned} 0 = \text{Im} & \left\{ \int_0^{R_w} r dr \int_0^\infty dI \int_0^{2\pi} d\psi \sum_{n, n'=-\infty}^{+\infty} e^{i(n-n')\psi} \right. \\ & \left. \times \left[\frac{\ell \frac{\partial f_0}{\partial p_\theta} - n \omega_b \frac{f_0}{T}}{n \omega_b + \ell \omega_E - \omega} \right] \delta H_{\ell, n'}^* \delta H_{\ell, n} \right\}. \end{aligned} \quad (\text{A5})$$

The ψ -integral gives the Kroenecker delta function $\delta_{nn'}$ and we have

$$0 = \text{Im} \left\{ \int_0^{R_w} r dr \int_0^\infty dI \sum_{n=-\infty}^{+\infty} \left[\frac{\ell \frac{\partial f_0}{\partial p_\theta} - n \omega_b \frac{f_0}{T}}{n \omega_b + \ell \omega_E - \omega} \right] |\delta H_{\ell, n}|^2 \right\}. \quad (\text{A6})$$

Setting $\omega = \omega_r + i\gamma_{\text{LD}}$ and expanding in the small quantity $\gamma_{\text{LD}}/\omega_r$ we obtain

$$\begin{aligned} 0 = \gamma_{\text{LD}} & \int_0^{R_w} r dr \int_0^\infty dI \\ & \times \sum_{n=-\infty}^{+\infty} \left[\frac{\ell \frac{\partial f_0}{\partial p_\theta} - n \omega_b \frac{f_0}{T}}{(n \omega_b + \ell \omega_E - \omega_r)^2 + \gamma_{\text{LD}}^2} \right] |\delta H_{\ell, n}|^2. \end{aligned} \quad (\text{A7})$$

For $\gamma_{\text{LD}} < 0$, the I -integral must be deformed into a contour that passes below the pole in accordance with Landau's initial value treatment. This procedure can be affected by replacing γ_{LD} with $|\gamma_{\text{LD}}|$ in the neighborhood of the pole. Integral (A7) can be divided into resonant and nonresonant contributions. For $\omega_b \gg \omega_E - \omega_r$, the nonresonant contribution will be dominated by the $n=0$ term,

$$\begin{aligned} 0 = \gamma_{\text{LD}} & \int_0^{R_w} r dr \int_0^\infty dI \frac{\ell \frac{\partial f_0}{\partial p_\theta}}{(\ell \omega_E - \omega_r)^2} |\delta H_{\ell, 0}|^2 \\ & + |\gamma_{\text{LD}}| \int_0^{R_w} r dr \int_0^\infty dI \\ & \times \sum_{n \neq 0} \left[\frac{\ell \frac{\partial f_0}{\partial p_\theta} - n \omega_b \frac{f_0}{T}}{(n \omega_b + \ell \omega_E - \omega_r)^2 + \gamma_{\text{LD}}^2} \right] |\delta H_{\ell, n}|^2, \end{aligned} \quad (\text{A8})$$

where the second integral is evaluated in the neighborhood

of the resonant points. We are considering a situation in which $\omega_r \neq \omega_E(r)$ anywhere inside the plasma, so that the first term is a proper integral. In the limit of small γ_{LD} , the second term in Eq. (A8) can be simplified using the following form of the Dirac delta function:

$$\lim_{\epsilon \rightarrow 0^+} \frac{\epsilon}{(x-y)^2 + \epsilon^2} = \pi \delta(x-y), \tag{A9}$$

and we find that

$$\gamma_{LD} = - \frac{\pi \int_0^{R_w} r dr \int_0^\infty dI \sum_{n \neq 0} \left[\ell \frac{\partial f_0}{\partial p_\theta} - n \omega_b \frac{f_0}{T} \right] |\delta H_{\ell,n}|^2 \delta[n \omega_b + \ell \omega_E - \omega_r]}{\int_0^{R_w} r dr \int_0^\infty dI \frac{\ell \frac{\partial f_0}{\partial p_\theta} |\delta H_{\ell,0}|^2}{(\ell \omega_E - \omega_r)^2}}, \tag{A10}$$

which is Eq. (48).

APPENDIX B: AXIAL DEPENDENCE OF MODE POTENTIAL

A direct solution of the complete 3D eigenvalue problem is a challenging numerical problem. Therefore, an iterative approach will be used to find an approximation of $\delta\phi_\ell(r,z)$ in the high bounce frequency limit ($\omega_b \gg \ell \omega_E - \omega$). Including axial dependence, the Poisson equation for the perturbations is

$$\left[\frac{1}{r} \frac{\partial}{\partial r} \left(r \frac{\partial}{\partial r} \right) - \frac{\ell^2}{r^2} + \frac{\partial^2}{\partial z^2} \right] \delta\phi_\ell(r,z) = 4\pi e \delta n_\ell(r,z). \tag{B1}$$

To get the density perturbation $\delta n_\ell(r,z)$, we note that there is a drift and an adiabatic contribution. From Eq. (13), the adiabatic contribution is given by

$$\delta n_\ell^{(a)} = \int_{-\infty}^{+\infty} dv \frac{e f_0(r,z,v)}{T} \delta\phi_\ell(r,z) - \int_{-v_s(r)}^{v_s(r)} dv \frac{e f_0(r,z,v)}{T} \langle \delta\phi_\ell(r,z) \rangle, \tag{B2}$$

where we have used $\langle \delta\phi_\ell \rangle = 0$ for passing particles. The first integral on the right hand side of Eq. (B2) is straightforward. However, the second integral cannot be evaluated without first obtaining $\delta\phi_\ell(r,z)$ which is not yet known. In order to simplify the calculation, we recall that the squeeze and end regions are small compared to the overall column length. To a good approximation we can use the infinitesimal squeeze region solutions found in Sec. IV for the bounce average potential, that is, $\langle \delta\phi_\ell(r,z) \rangle \approx \delta\phi_\ell(r)$, where $\delta\phi_\ell(r)$ is a solution to Eq. (27). Thus, the adiabatic density perturbation is

$$\delta n_\ell^{(a)} = \frac{e n_0(r,z)}{T} \delta\phi_\ell(r,z) - \frac{e n_t(r,z)}{T} \delta\phi_\ell(r). \tag{B3}$$

The drift perturbation can be found by considering the change in the number of trapped particles on a field line due to the presence of the mode. Again, we make the approximation $\langle \delta\phi_\ell(r,z) \rangle \approx \delta\phi_\ell(r)$ and obtain the radial displacement of the trapped particles $\Delta r = -c\ell \delta\phi_\ell(r)/Br\omega'(r)$. The associated density perturbation due to drift motion is

$$\delta n_\ell^{(d)} = n_t(r - \Delta r, z) - n_t(r, z) = \frac{c\ell}{Br} \frac{\partial n_t(r,z)}{\partial r} \frac{\delta\phi_\ell(r)}{\omega'(r)}, \tag{B4}$$

where $\omega'(r) = \ell \omega_E(r) - \omega$ and ω is given in the solution of Eq. (27). Of course, the passing particles have no bounce average drift perturbation.

Substituting the total density perturbation into Poisson’s equation yields the equation

$$\left\{ \frac{1}{r} \frac{\partial}{\partial r} \left(r \frac{\partial}{\partial r} \right) - \frac{\ell^2}{r^2} + \frac{\partial^2}{\partial z^2} \right\} \delta\phi_\ell(r,z) - \frac{4\pi e^2 n_0(r,z)}{T} \delta\phi_\ell(r,z) = \left[\frac{4\pi e c \ell}{Br \omega'(r)} \frac{\partial n_t(r,z)}{\partial r} - \frac{4\pi e^2 n_t(r,z)}{T} \right] \delta\phi_\ell(r). \tag{B5}$$

For consistency, we verify that $\delta\phi_\ell(r,z) = \delta\phi_\ell(r)$ inside the main column by setting them equal in Eq. (B5) and noting that Eq. (27) is recovered. The radial boundary conditions on Eq. (B5) are $\delta\phi_\ell(0,z) = \delta\phi_\ell(R_w,z) = 0$. Further, $\delta\phi_\ell(r,0) = 0$ because the mode is odd about $z=0$. At large z , the mode potential decays exponentially and we impose the condition $\delta\phi_\ell(r,L_\infty) = 0$, where L_∞ is suitably larger than L . Equation (B5) is discretized and solved directly by matrix inversion.

¹A. A. Kabantsev, C. F. Driscoll, T. J. Hillsabeck, T. M. O’Neil, and J. H. Yu, Phys. Rev. Lett. **87**, 225002 (2001).
²W. M. Tang, Nucl. Fusion **18**, 1089 (1978).
³G. A. Navratil, A. K. Sen, and J. Slough, Phys. Fluids **26**, 1044 (1983).
⁴M. N. Rosenbluth, D. W. Ross, and D. P. Kostomarov, Nucl. Fusion **12**, 3 (1972).
⁵M. Rosenbluth, W. M. MacDonald, and D. L. Judd, Phys. Rev. **107**, 1 (1957).
⁶D. Montgomery, G. Joyce, and L. Turner, Phys. Fluids **17**, 2201 (1974).
⁷C. F. Driscoll, Phys. Rev. Lett. **64**, 645 (1990).
⁸A. A. Kabantsev (private communication, 2002).
⁹L. D. Landau and E. M. Lifshitz, *Fluid Mechanics* (Pergamon, Oxford 1979), p. 228.
¹⁰X. P. Huang, F. Andereg, E. M. Hollmann, C. F. Driscoll, and T. M. O’Neil, Phys. Rev. Lett. **78**, 875 (1997).
¹¹A. A. Kabantsev and C. F. Driscoll, Phys. Rev. Lett. **89**, 245001 (2002).
¹²T. J. Hillsabeck and T. M. O’Neil, Phys. Plasmas **8**, 407 (2001).